NOTICE

The quality of this microform is heavily dependent upon the quality of the original thesis submitted for microfilming. Every effort has been made to ensure the highest quality of reproduction possible.

If pages are missing, contact the university which granted the degree.

Some pages may have indistinct print especially if the original pages were typed with a poor typewriter ribbon or if the university sent us an inferior photocopy.

Reproduction in full or in part of this microform is governed by the Canadian Copyright Act, R.S.C. 1970, c. C-30, and subsequent amendments.

AVIS

La qualité de cette microforme dépend grandement de la qualité de la thèse soumise au microfilmage. Nous avons tout fait pour assurer une qualité supérieure de reproduction.

S'il manque des pages, veuillez communiquer avec l'université qui a conféré le grade.

La qualité d'impression de certaines pages peut laisser à désirer, surtout si les pages originales ont été dactylographiées à l'aide d'un ruban usé ou si l'université nous a fait parvenir une photocopie de qualité inférieure.

La reproduction, même partielle, de cette microforme est soumise à la Loi canadienne sur le droit d'auteur, SRC 1970, c. C-30, et ses amendements subséquents.

UNIVERSITY OF ALBERTA

Digital Analysis of Low-Relief Topography

in a Landsat Snow-Cover Scene

in South-Central Alberta

by

K. Robert Shoye

Ⓒ

A THESIS

SUBMITTED TO THE FACULTY OF GRADUATE STUDIES AND RESEARCH

IN PARTIAL FULFILMENT OF THE REQUIREMENTS FOR THE DEGREE OF

Master of Science

Department of Geography

Edmonton, Alberta

Fall, 1990

UNIVERSITY OF ALBERTA

RELEASE FORM

NAME OF AUTHOR   Kenneth Robert Skoye

TITLE OF THESIS   Digital Analysis of Low-Relief Topography in a Snow-Cover Landsat Scene in South-Central Alberta

DEGREE FOR WHICH THESIS WAS GRANTED   Master of Science

YEAR THIS DEGREE GRANTED   1990

Permission is hereby granted to THE UNIVERSITY OF ALBERTA LIBRARY to reproduce single copies of this thesis and to lend or to sell such copies for private, scholarly or scientific purposes only.

The author reserves other publication rights, and neither the thesis nor extensive extracts from it may be printed or otherwise reproduced without the author's written permission.
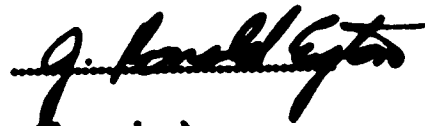
(SIGNED) ....

P.O. Box 956
Chisholm, Alberta
Canada T0L 0T0

DATED 22/23, 1990

THE UNIVERSITY OF ALBERTA

FACULTY OF GRADUATE STUDIES AND RESEARCH

The undersigned certify that they have read, and recommend to the Faculty of
Graduate Studies and Research, for acceptance, a thesis entitled Digital Analysis of
Low-Relief Topography in a Landsat Snow-Cover Scene in South-Central Alberta
submitted by K. Robert Shoye in partial fulfilment of the requirements for the degree
of Master of Science.

....
(Supervisor)

....

....

DATED ....Jan. 4. 19 ...82...

dedicated to the memory
of my late Grandfather and friend

HERBERT ENTICKNAP

ABSTRACT

Digital radiometric enhancement of low-relief topographic expression in a January 14, 1984, Landsat Multispectral Scanner System scene revealed extensive areas of unmapped glacigenic terrain in south-central Alberta. The reflectance properties of snow-covered surfaces illuminated at a low, mid-winter solar elevation produced measurable image brightness differences from slope variations as small as 0.28 degrees. These slight differences were utilized to detect and enhance glacial meltwater channel networks and large-scale, low-relief flutings. Image processing of the Landsat data produced synoptic views of accentuated topographic expression at various scales. Such expression is poorly recorded, if at all, by conventional aerial photography. Image enhancement techniques that proved to be effective with snow-covered topography included linear contrast stretching with saturation, image inversion and principal components transformation. Colour composites of contrast stretched bands 4,5 and 7 showed considerable colour differences for a snow-cover scene in addition to emphasizing the apparent texture of various ground cover types. The results of this study have shown that snow-covered terrain, illuminated at a low solar elevation in a Landsat scene, produced image data sets that were effectively enhanced to reveal very low-relief, large-scale landform structures and patterns on a prairie landscape.

v

ACKNOWLEDGEMENTS

TABLE OF CONTENTS

LIST OF TABLES

LIST OF FIGURES

LIST OF PLATES

I. INTRODUCTION

Background

The presence of snow upon the landscape naturally enhances terrain forms and patterns. Various researchers have utilized the reflectance characteristics of snow-covered surfaces, in combination with the synoptic view of the earth afforded by satellite imagery, for terrain and natural resource studies. Delineation of geologic fractures and lineaments (Wobber and Martin, 1973, 1974), identification of wildlife habitat (Crooks, 1968; Jacques, 1982) and delineation of general topographic expression (Morrison, 1976; Wobber and Martin, 1973, 1974) have been accomplished using snow-cover satellite imagery. These previous studies utilized snow-cover scenes primarily because of the differential accumulation or depletion of snow over the earth's surface, the reduction of visually confusing colour variations from vegetated and bedrock/soil surfaces, and because of the increased tonal contrast resulting from low solar elevations and the resulting elongated shadows.

The detection and mapping of landforms and surficial deposits associated with continental ice-sheet development on the southern Alberta prairie has traditionally been undertaken using aerial photograph analysis and intensive field investigation (for example, see Shetsen, 1987, 1990; Smith, 1987; Stalker, 1960 a,b, 1973; Tsui et al, 1989). Although snow-cover imagery has been used by some authors to illustrate small landforms up to hundreds of square metres in area from aerial photos (Beaty, 1975), no specific studies have been carried out utilizing snow-cover satellite imagery to

1

detect and enhance large landform structures and patterns of the Alberta prairie environment. Eyton (1989) demonstrated the effectiveness of such imagery in highlighting extensive systems of glacial moraines, with average slope inclinations of approximately one degree, in central Illinois. By modelling the reflectance of low-relief, snow-covered topography in a Landsat scene, Eyton (1989) provided a basis for effectively enhancing low-relief topographic expression in a Landsat scene.

Objectives

The primary objective of this research was the enhancement of low-relief topographic expression at a regional scale in southern Alberta using a snow-cover Landsat scene. Conventional image processing techniques were used to develop enhanced scene products. The reflectance properties of the snow-covered surfaces in the scene were determined and evaluated. The model was utilized to predict pixel brightness values representing subtle slope facet differences.

The potential for utilizing enhanced Landsat snow-cover imagery for detecting extensive physiographic structures and patterns at a synoptic scale was also assessed. The enhanced imagery was expected to reveal subdued, but areally extensive, landforms created by the thick Laurentide ice sheet (Dyke and Prest, 1987) and/or large volumes of sub-glacial meltwater (Shaw et al, 1989). Glacial landforms of the prairies provide geomorphic clues as to the thicknesses and dynamics of continental ice as it approached and wasted from Late Wisconsinan limits (Burns and Young, 1988; Campbell, 1987; Dyke and Prest, 1987; Rains et al, 1990).

II. DATA AND STUDY AREA

Data

The digital image data used in this study were acquired by the Landsat 4 multispectral scanner system (MSS) sensor on January 14, 1984, at 9:51 a.m. local time (Table 1). The computer-compatible tape of the full-scene image was obtained from the Canada Centre for Remote Sensing at Prince Albert, Saskatchewan. All four MSS bands (4,5,6 and 7) were unpacked for spectral analysis; destriping and geometric correction processing of the image data were done at Prince Albert. Figure 1 shows the footprint of the full Landsat scene and two extracted subscene images. Image processing of the MSS data was completed at the University of Alberta using a Decision Images processing system and software developed in the Department of Geography's Computer Cartography Laboratory. Photographs of processed image subscenes were obtained using 100 ISO colour negative film and black and white negative film with a 35 millimetre format Dunn Camera system.

Study Area

The footprint of the full Landsat scene area (Figure 1) is located within the Interior Plains region of western Canada (Pettapiece, 1986) in south-central Alberta. Located north-northeast of Calgary, this area (approximately 185 x 185 kilometres) is bisected by the deeply incised Red Deer River valley from northwest to southeast. Physiographic variations in this area result primarily from the combined influences

3

Table 1. Image Data Specifications

Satellite:	Landsat 4
Sensor:	Multispectral Scanner System
Spatial Resolution:	57 metres wide x 82 metres long
Spectral Resolution:	0.5-1.1 um in four bands
Product Type:	System Georeferenced
Location:	Path 41/Row 24
Scene Centre Time:	1984-01-14; 9:51 a.m. local time
Scene Centre Latitude:	51.689 degrees north
Scene Centre Longitude:	112.367 degrees west
Sun Elevation:	13.49 degrees
Sun Azimuth:	154.55 degrees
Scene Coverage:	185 kilometres x 185 kilometres
Cloud Cover:	Minimal; less than 10%
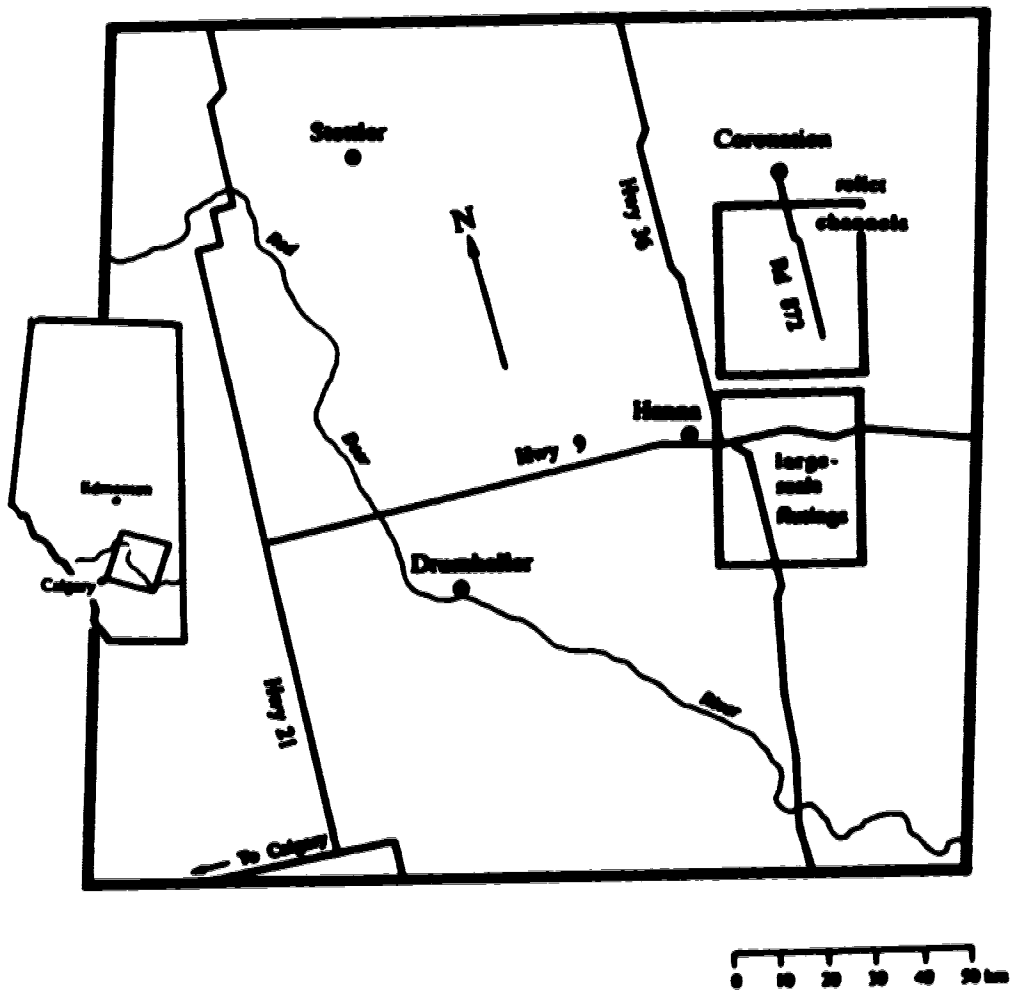
Figure 1. Landsat image footprint over south-central Alberta and the two selected image subscenes.

of Tertiary fluvial dissection of bedrock, Pleistocene glacial sedimentation and Holocene fluvial incision. These semi-arid and generally treeless plains are underlain dominantly by Upper Cretaceous and Tertiary sandstones and shales veneered with varying thicknesses of Quaternary glacigenic debris (Shetsen, 1987, 1990; Stalker, 1960, 1973). The region displays a relatively flat to gently undulating topography. Notable areas of more obvious relief are the Hand Hills and neighbouring Wintering Hills (found in the central portion of the study area) and the Neutral Hills in the extreme northeastern corner. These highlands rise 100 to 200 metres above the surrounding prairie surfaces.

Although much of the region's geomorphology and geology has been mapped (Irish, 1967; Shetsen, 1987, 1990; Stalker, 1960 a,b, 1973), some terrain suites, including large-scale flutings and ancient meltwater channel systems, visible in the Landsat snow-covered scene, have escaped previous detection and accurate identification. Because of their often subtle relief, and relatively large areal extents, these structures show little or no apparent topographic expression to the field investigator or on conventional aerial photographs. Low-relief, erosional landforms of this subdued nature characterize substantial portions of the study area, and probably reflect Pleistocene, glaciofluvial formation processes that episodically affected vast expanses of the interior plains. The maps of Shetsen (1987, 1990) clearly support this connection.

Two Landsat snow-cover subscenes were chosen for analysis because they contained such distinctive landforms not identified or mapped previously. Apparent in

the first subscene are enormous and elongated "island" forms (up to five kilometres long) and meltwater channel systems extending at least tens of kilometres. Some of the larger relict glacial meltwater channels are shown on Shetsen's (1990) map of central Alberta. A second subscene, south of the relict channels area, was selected for low-relief topographical enhancement because of the extensive "corrugated" appearance of the prairie surface. The parallel, to partially divergent and convergent, "fluted" forms, are often over thirty kilometres long and a kilometre wide (measured from one "ridge" top to the next). These intriguing features are not shown on existing surficial geology maps of the area (see Shetsen, 1987 for example). The subscene of relict glacial meltwater channels and large-scale flutings were thus selected for enhancement of their low-relief topographic expression because of their potential for geomorphological interpretation.

III. ENHANCEMENT OF A SNOW-COVER SCENE

A goal of image enhancement is to improve the visual interpretability of the image by increasing the apparent distinctions between features in the scene (Lillesand and Kiefer, 1987). Computer processing of Landsat MSS digital image data allowed for the selective numerical manipulation of pixel brightness values which comprise a Landsat image data set. These values represent electromagnetic radiation intensities reflected from the surface of the earth and recorded by the MSS sensor. This section of the thesis outlines the digital image processing techniques used to enhance digital subscenes extracted from the Landsat snow-cover scene. A more general treatment of image processing methods can be found in Lillesand and Kiefer (1987) and Richards (1986).

Image Processing of a Snow-Cover Scene

Linear Contrast Stretching with Saturation

Contrast stretching is a radiometric enhancement procedure whereby the range of brightness intensities, or grey levels, in an image is increased. Image data subsets of unenhanced, snow-cover images not spanning the entire grey scale for the MSS electronic sensor generally displayed a limited range of brightness levels, resulting in a low scene contrast (Plate 1). The radiometric, or tonal quality of sampled single band image subsets was assessed from scene histograms. Band 6 data were selected because of the greater dynamic brightness range as indicated by the histogram shown in Figure

8

2. Digital contrast stretching expanded the linear range between pixel grey level values to match the maximum computer screen brightness range. Clipping of each tail of the grey level distribution was done in order to maximize tonal contrast of the image while minimizing the loss of brightness information within the scene. A 2.5% clipping of the grey level values at the lower end of the stretched distribution caused largely snow-free, heavily vegetated, or shadowed areas to appear black in the resulting image, and those pixels representing the upper 2.5% of the grey level value distribution to saturate as white (Plate 2).
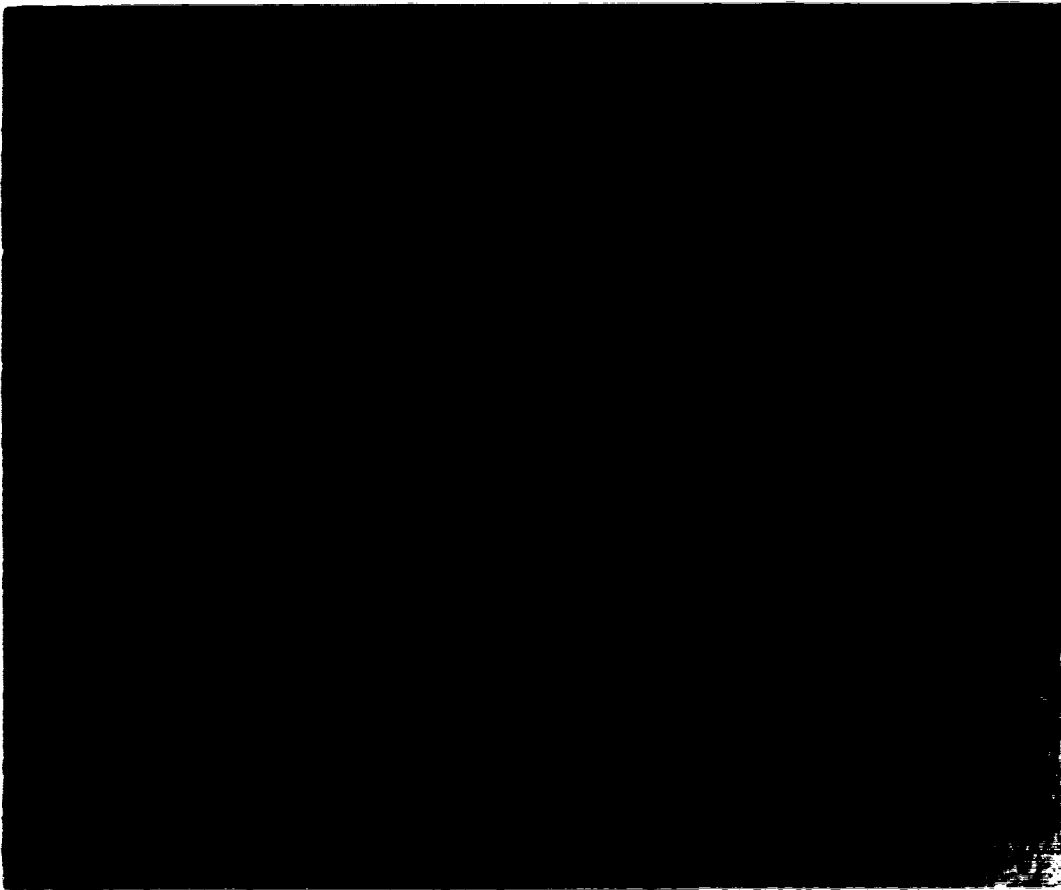
Plate 1. Unenhanced 512x512 pixel band 6 digital image subscene showing relict glacial meltwater channels and modified "island" forms.
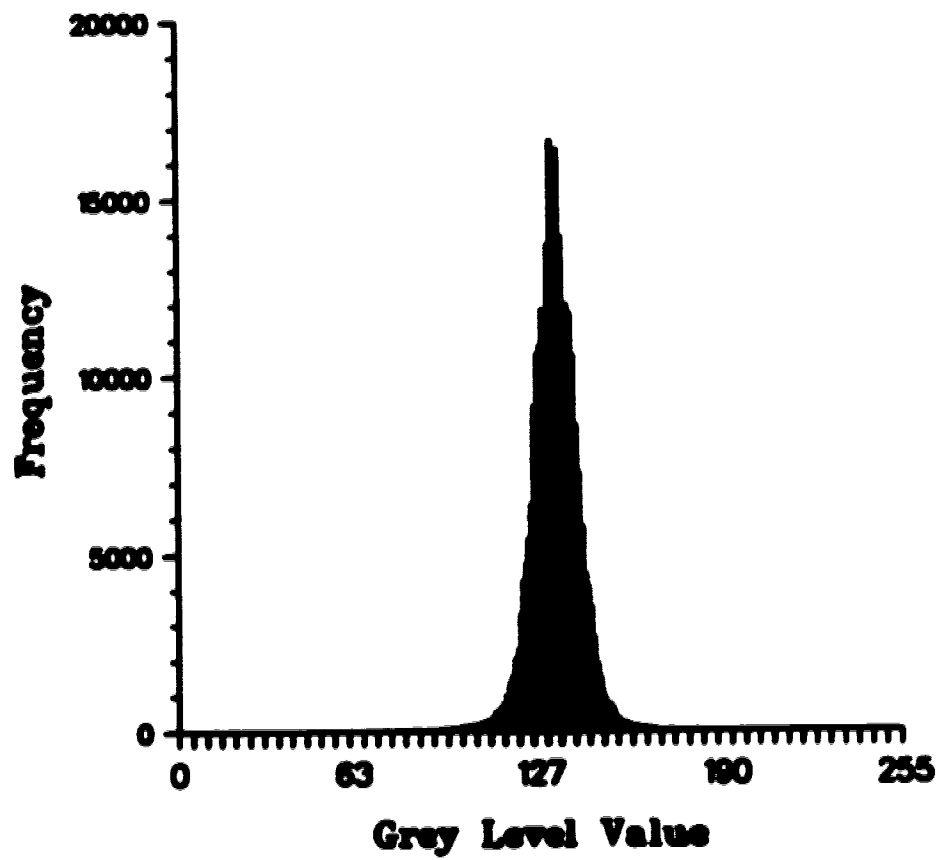
Figure 2. Histogram for the band 6 digital image subscene. Grey level value minimum=69 and grey level maximum=234.

Plate 2. Contrast stretched, band 6 image subscene with 2.5% of each tail of the grey level value distribution saturated black and white to increase tonal contrast.

Image Inversion

The differential illumination of topography produces shading depth clues from which the human visual system is able to perceive shape, pattern and relief in a monoscopic image (von Gunn, 1969). A low solar elevation at the time of image acquisition allowed for the detection of subtle landform expression within the study scene. Differential lighting and shading of slopes created small yet measurable variations in scene radiance reflected from the surfaces and recorded by the MSS sensor. Corresponding pixel brightness values, each representing both the reflectance properties and geometry of the snow-covered landscape units, comprised the data from which perception of complex landform structure was made possible in an enhanced image display (Eyton, 1969).

Although the human visual system is able to interpret shading depth clues and thus recover the three-dimensional shape of objects by using perceived variations in image intensity (Horn, 1982; Ramachandran, 1988), the real orientation, or geometry, of topographic features in an image is not always so readily apparent. The direction of lighting in an image during data acquisition is usually a critical component in human visual perceptions of positive and negative relief elements from that image. Multispectral scanner system scenes in the northern hemisphere are illuminated from the southeast, which often results in the appearance of inverted relief, a confusing phenomenon often encountered by air photo interpreters (Smith, 1943). Plate 2 is a normal contrast stretched image subset with the sun illuminating the scene from the southeast. Interpretation confusion may arise regarding the real orientation of the

convex "island" forms visible in the image, or the negative relief stream valleys visible in the southwestern corner of the image subscene. Owing to the small relative relief of the study area topography, this phenomenon of inversion is not as obvious nor consistent to viewers as in images of more rugged terrain (for example, see Evans, 1990).

Re-orientating the apparent direction of illumination from the southeast to the northwest ensures that most people will see the true geometric nature of the landscape features in the enhanced image subscenes. Altering this apparent direction of the sun's illumination was accomplished by simply inverting the grey scale of the image (after von Gara, 1989). Inversion was obtained by subtracting the pixel grey level value, or digital number (DN) from 255 in the enhanced data set, producing a "negated" image. Plate 3 is a digitally inverted, contrast stretched image resulting in topography that is more readily perceived than in the non-inverted image subscene. Snow-cover scenes are particularly amenable to inversion of the grey scale because of their monochromatic appearance. Negating an essentially white image results in a more familiar darkened image (with respect to summer images) with the apparent source of illumination located in the northwest. The inverted image closely resembles an image acquired by radar (see Smith, 1987, pp. 42 and 85).
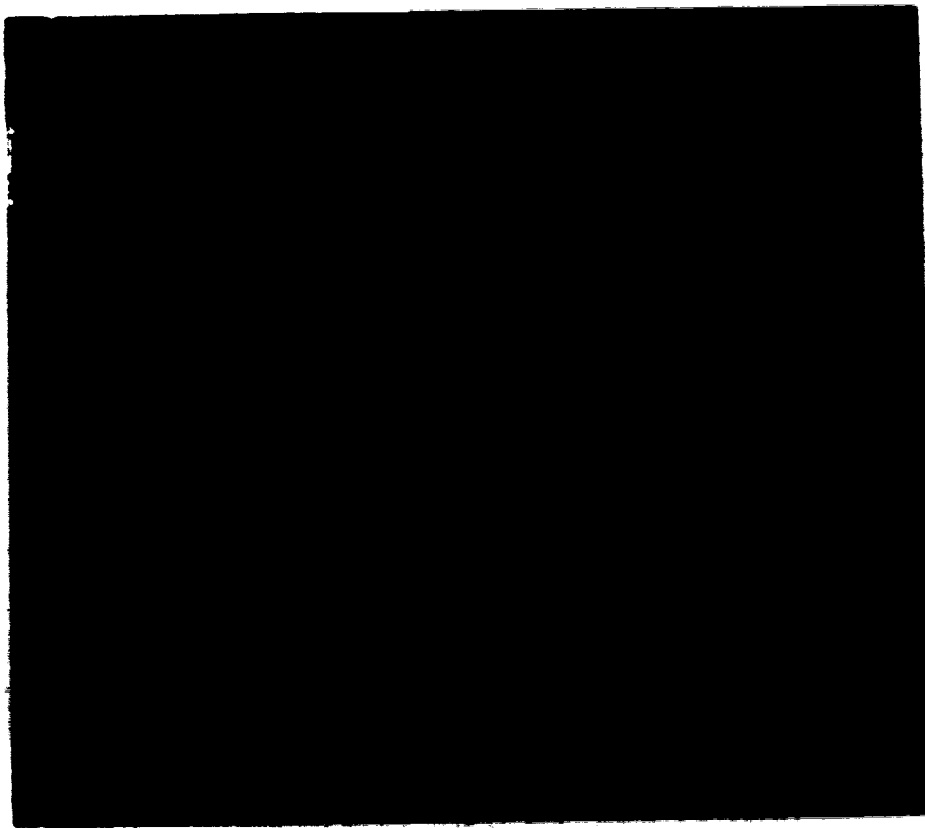
Plate 3. Digitally inverted, contrast stretched band 6 image subset in which concavity and convexity of topographic features is more readily perceived than in Plate 2.

Colour Compositing

Multi-band image compositing of MSS data produced colour image subsets of snow-covered and snow-free terrain within the study area. False colour composites of band 4 (green), band 5 (red) and band 7 (infrared) responses showed considerable tonal differences, and emphasized the textures of various snow-covered surface types. Loss of spectral information due to sensor saturation was not significant in much of the Alberta Landsat image as encountered in MSS images of Antarctica (Lucchita et al, 1987).

False colour composite images were produced by displaying the individually contrast stretched bands 4,5 and 7 as blue, green and red images respectively on the output display screen. Plate 4 shows the resulting false colour composite image with the source of illumination located in the southeast. Plate 5 is the inverted false colour composite image that conveys the "normal" topographic orientation of geomorphic features within the subscene. Note that inverting the grey scale of each band results in a composite image that is displayed in colours that are complementary to the colours of the original composite. Inversion of the image colours was not detrimental to the recognition of the topography; morphological distinction has been increased and the colours of the false colour images do not correspond to the expected natural colours of the reflecting surfaces in either case.

Plate 4. Contrast stretched, false colour composite image with bands 4,5 and 7 assigned to the blue, green and red guns respectively.
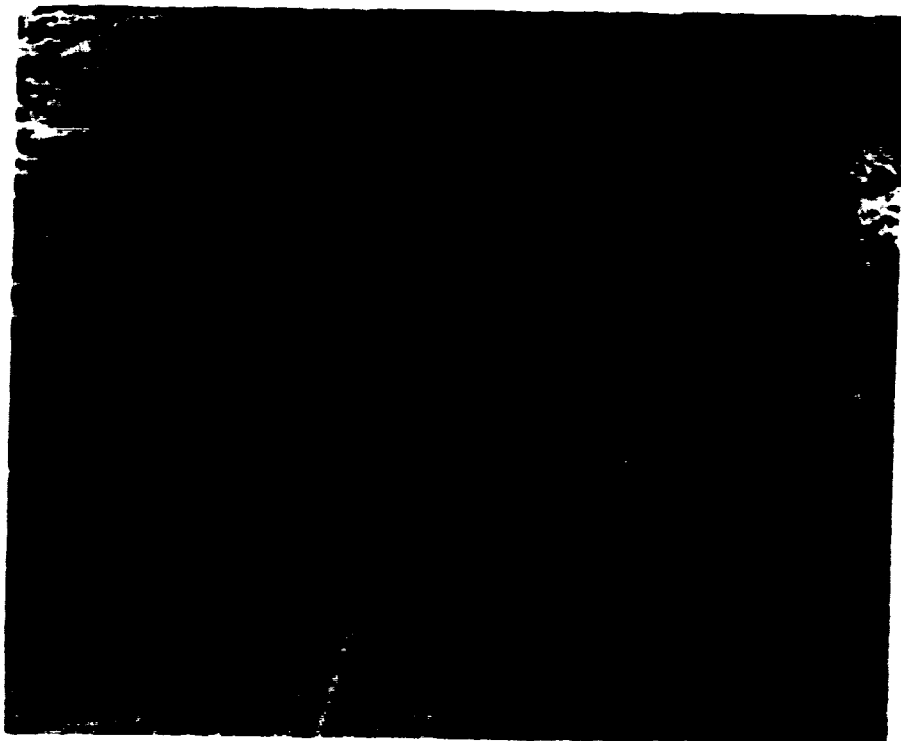
Plate 5. Inverted and contrast stretched, false colour composite image with the apparent source of illumination flipped to the northwest.

Principal Components Analysis

Display of single band image subsets from bands 4,5,6 and 7 of the MSS image data resulted in snow scene images very similar in appearance. Principal components analysis (PCA) was employed to assess the correlation between the recorded radiance from the four MSS spectral bands in a snow-cover digital subscene. PCA images were generated from mathematically transformed grey level values comprising the original subset image data; see Davis (1986) for a detailed description of the statistical procedures used to derive principal component transformations.

Measured similarity between the pixel radiance values from all four MSS spectral bands for a selected image subset is numerically described by the correlation matrix in Table 2. Most obvious from the matrix is the high relative correlation between visible and infrared bands. This correlation indicates similar visible and infrared spectral reflectance intensities from the snow-covered surfaces recorded by the MSS sensor. The smallest correlation exists between the green and infrared bands, indicative of their relative distance apart on the electromagnetic spectrum. MSS band 6 was the most highly correlated band with regard to the brightness values from the other three spectral bands. These correlations are unusual compared to summer imagery where visible light is usually not correlated with infrared spectral responses.

Table 2. Principal Components Analysis Results

Correlation Matrix

	B4	B5	B6	B7
B4	1.0000	0.8040	0.8142	0.7803
B5	0.8040	1.0000	0.8535	0.8266
B6	0.8142	0.8535	1.0000	0.8605
B7	0.7803	0.8266	0.8605	1.0000

Eigenvalues

	Eigenvalue	Proportion	Cumulative
PC1	3.47021	0.867554	0.86755
PC2	0.22888	0.057219	0.92477
PC3	0.16978	0.042446	0.96722
PC4	0.13112	0.032781	1.00000

Eigenvectors

	PC1	PC2	PC3	PC4
B4	0.489028	0.836485	0.223978	0.104778
B5	0.502202	-.110205	-.812901	0.273570
B6	0.508800	-.209936	0.062612	-.832544
B7	0.499767	-.494040	0.533853	0.470162

Eigenvalues representing the proportion of total brightness data variance contained in PC images 1,2,3 and 4 are shown in Table 2. PC1 image explains most (86.7%) of the variance from all four bands. Inspection of the corresponding transformed PC1 image (Plate 6) subscene shows its similarity to the contrast stretched band 6 image (Plate 2). The PC1 image, however, contains mostly brightness information from all four MSS sensor bands; the eigenvectors (principal component transformation coefficients, or "loadings") listed in Table 2 show that PC1 is weighted nearly equally with respect to input from all four MSS bands. PC2 and PC3 images (Plates 7 and 8) show considerable noise; these two transformations explain only 5.7% and 4.2% of the variance respectively and according to the eigenvectors show visible contrasts or differences with respect to the far infrared band 7. PC4, although explaining the least amount of variance (3.3%), does show some fluting detail. The eigenvector for PC4 indicates a band 6 versus all other bands contrast with the largest difference occurring for band 7. Sun-facing and sun-opposing radiance differences may be responsible for the contrast.

Plate 6. Principal component 1 image displaying 96.7% of the explained spectral variance in bands 4,5,6 and 7. Eigenvector loadings indicate brightness, or intensity, as the dominant response.

Plate 7. Principal component 2 image displaying only 5.7% of the explained variance according to the eigenvectors in Table 2.

Plate 8. Principal component 3 image displaying only 4.2% of the explained variance according to the eigenvectors in Table 2.
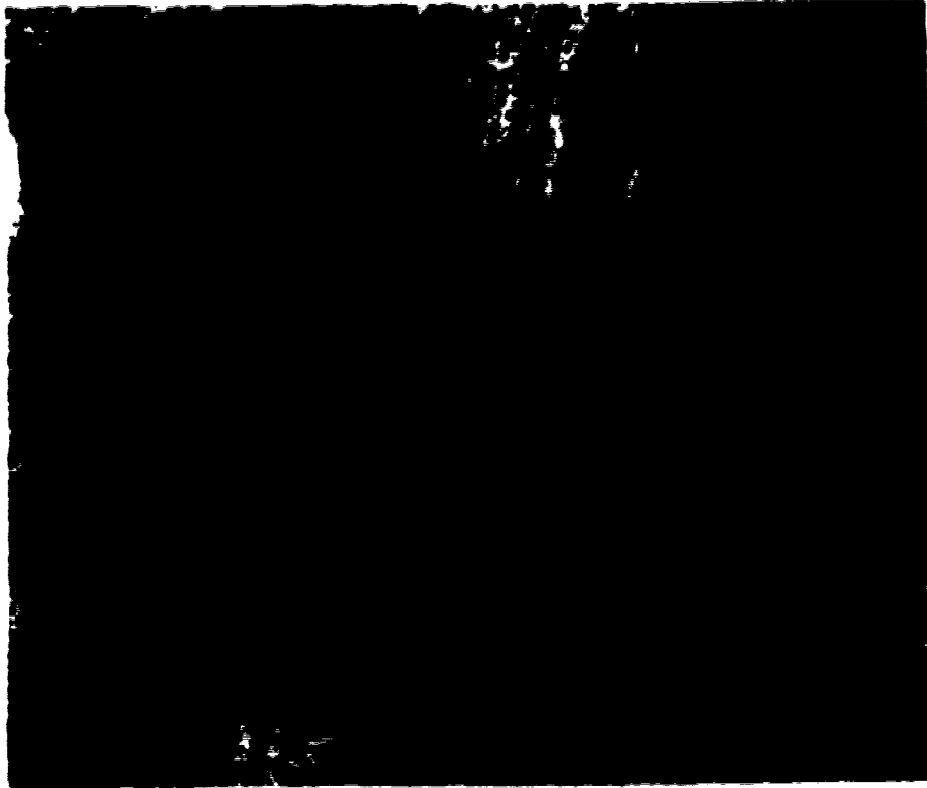
Plate 9. Principal Component 4 image displaying the least amount of explained variance (3.9%).

General Interpretation of Low-Relief Topography

<u>Relict Meltwater Channels</u>

Digital enhancement of low-relief, snow-covered topography effectively delineated discrete and extensive relict meltwater channel systems and residual "islands" visible in Plate 10. These remnant features appear to reflect former glacial meltwater flows from northwest to southeast, either as sub-aerial (proglacial or ice-marginal) channels, or large-scale, partly channelized, sub-glacial sheet flows. At least two scales of meltwater channels are visible in the enhanced subscene. Relatively narrow channels flank the elongated, streamlined, residual "islands" that are up to one kilometre wide and five kilometres long. Broader channels, up to five kilometres wide in the subscene, appear to partially truncate some residual "islands" and have both contributory and distributary linkages with the narrower systems (Rains, pers. comm.).

Casual field inspection of the subscene area showed the channels and "island" structures to be largely water-eroded bedrock surfaces with gently undulating topography (Plate 11) and frequent occurrence of lag boulders. Concentrations of poorly sorted coarse gravel and sand were observed within parts of the larger channels (Plate 12). Some of these channels and deposits were mapped by Shetsen (1990), at 1:500,000 scale, using conventional aerial photograph analysis and field investigation. Absent from Shetsen's map, however, are the geomorphic details of system morphologies evident in the enhanced satellite imagery. The sub-parallel patterns of the narrower channels and the related, elongated, residual bedrock "island" forms suggest formation of these structures under high energy glaciofluvial flow conditions.

26
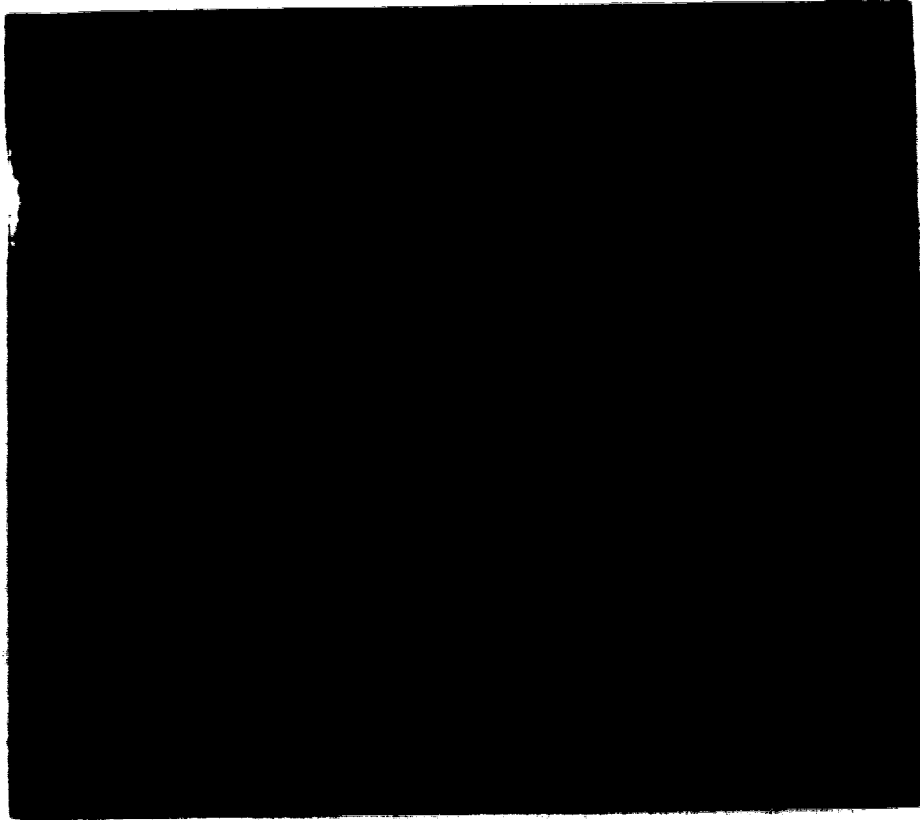
Plate 18. Contrast stretched and inverted band 6 glacial meltwater channel subscene south of Coronation (Figure 1) showing channels and residual "islands".

Plate 11. Ground view of undulating meltwater channel topography near secondary road 872 south of Coronation (Figure 1).
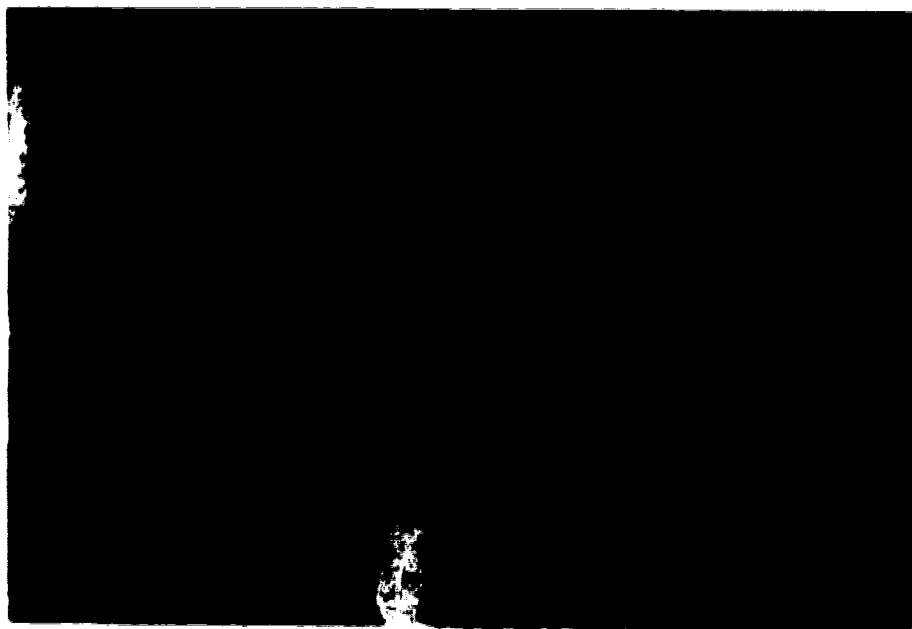
Plate 12. An example of a coarse gravel deposit located in parts of the broad, residual channels visible in Plate 10.

A speculative explanation of their genesis lies in applications of subglacial,
catastrophic sheet-flood theories presently being developed (see, for example, Shaw et
al, 1989). Such applications, while beyond the immediate scope of this thesis, may
prove to be the focus of related, future studies.

Large-Scale Flutings

A series of elongated ridge and trough forms over an area approximately 30
kilometres long and 20 kilometres wide are visible in Plate 13. Located east of the
town of Hanna (Figure 1), the sub-parallel flute features trend in a southwesterly
direction, are cross-cut by relict channels to the north, and abruptly terminate to the
south in an amorphous zone also visible in Plate 13. These large-scale flutings are not
visible on existing aerial photographs of the area. Casual field inspection showed the
fluting ridges and troughs to be eroded in Cretaceous, sedimentary bedrock. No
significant cover of glacial till was observed within the area. Poorly sorted gravel and
sand units, however, were found in a broad meltwater channel complex southeast of
the main fluting field (Plate 14). Measured distances between adjacent fluting crests
varied up to several hundred metres, with local relief, between crests and troughs, up
to three metres. Surface slopes were estimated to range generally up to a maximum of
about two degrees. Plate 15 is a photograph looking directly west across the flutings
south of highway 9 (Figure 1). The very subtle topographic expression of the flutings
is reflected by the slight undulations of the power poles in the near and far distance.
Plate 16 shows an unusually steep slope facet of one of the most prominent flutings
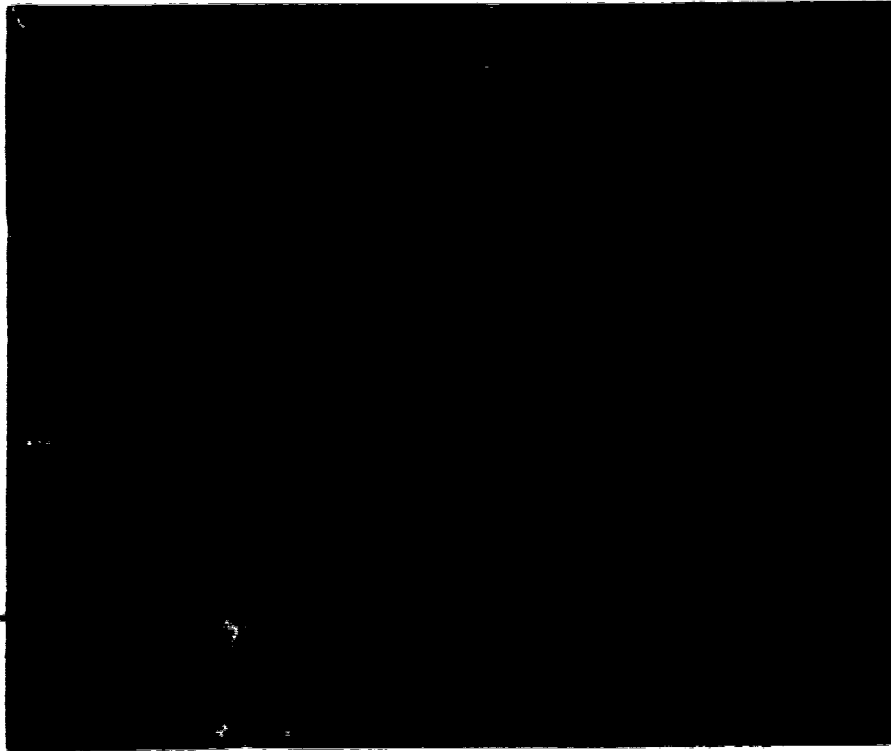
Plate 13. Contrast stretched and inverted band 6 image east of Hanna (Figure 1) showing low-relief, large-scale findings.
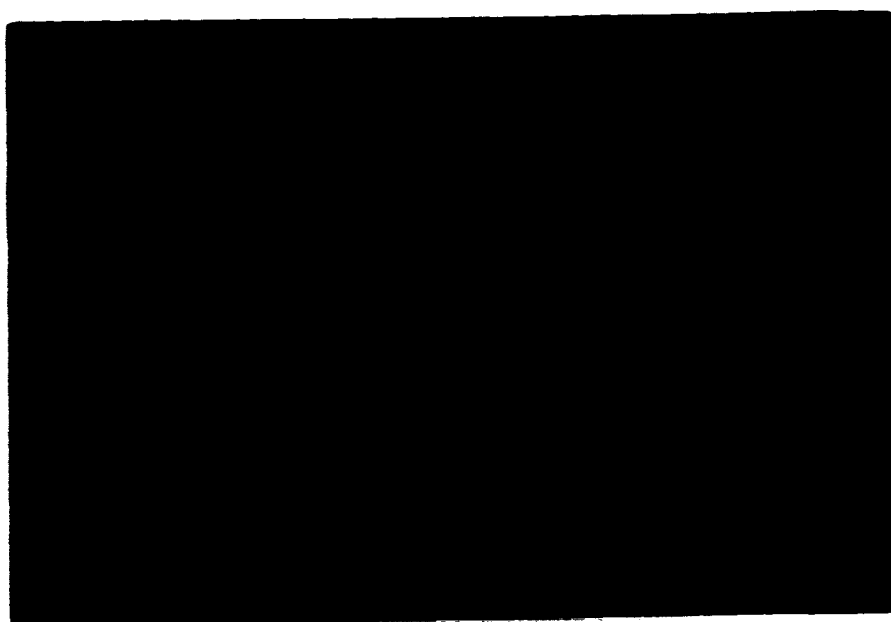
Plate 14. An example of poorly sorted gravels and sands in part of the bedrock complex southeast of the main fluting field in Plate 13.

southeast of Hanna.

Elongated in the assumed direction of ice flow, flutings in western Canada have usually been interpreted by investigators to result directly from thick ice sheets sliding over underlying sediments and/or bedrock, physically deforming and/or eroding the subglacial materials (Gravenor and Meneley, 1958; Jones, 1982; Moran et al, 1980; Shaw, 1975, 1980; Smith, 1948; Stalker, 1960 a,b, 1973). A more recent theory attributes formation of large-scale flutings, some types of drumlins, some types of meltwater channels and related sediments to enormous, episodic, catastrophic discharges of subglacial sheet-floods with subsequent, waning, tunnel-valley flows (Shaw and Kvill, 1984; Shaw and Sharpe, 1987; Shaw et al, 1989). The large-scale flutings discussed in this study are comparable in wavelength (but much smaller in wave height) to flutings near Athabasca, north-central Alberta, which show morphological and sedimentological characteristics vindicating the massive, episodic, sheet-flood hypothesis (Shaw et al, in prep.). The apparent water-scoured nature of the large-scale Hanna flutings suggests that they were also formed by glaciofluvial erosion. The markedly lower relief of the Hanna flutings in comparison to the Athabasca flutings, 360 kilometres to the north, may be indicative of different volumes/pressures of their respective, hypothetical sheet-floods, but with fundamentally similar secondary flows (Rains, pers. comm.). Certainly, more intensive investigations of these previously undetected flutings (and other distinctive, related Laurentide landforms) are warranted.
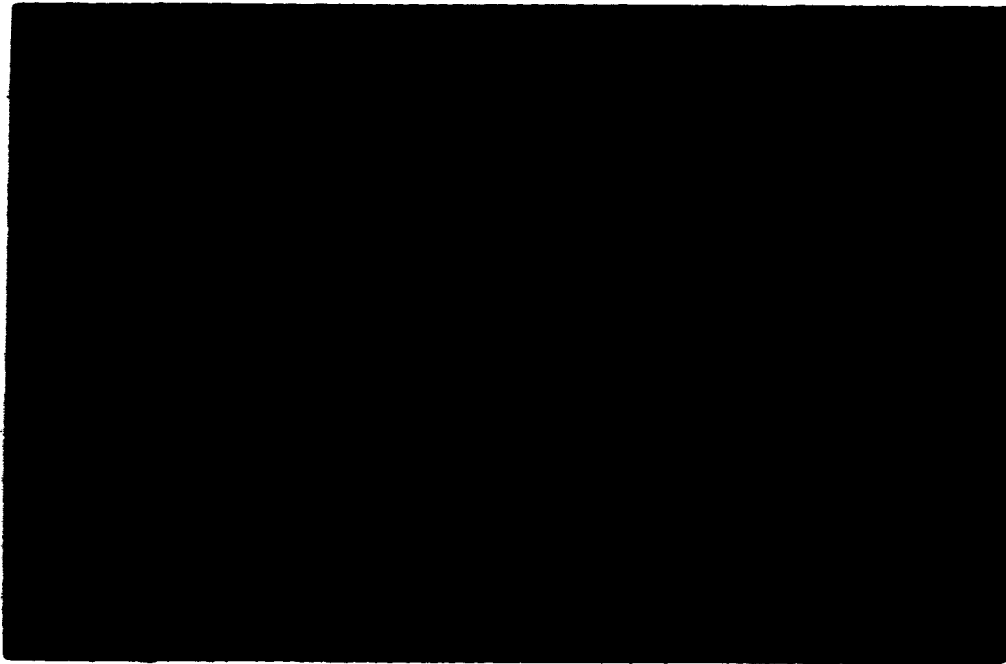
Plate 15. Looking west directly across the findings. Subtle topographic expression of findings is indicated by the slight undulations of power poles in the near and far distance.

Plate 16. A fluting slope southeast of Husum (Figure 1).

IV. REFLECTANCE MODELLING OF A SNOW-COVER SCENE

Reflectance Functions

All natural surfaces have preferred orientations of light scattering (Kreibel, 1978), and are thus satisfactorily modelled by a non-diffuse reflectance model (Justice et al, 1981). A photometric function proposed by Minnaert (1941) was used in this analysis to model the brightness, or reflectance, of snow-covered surfaces in a Landsat snow-cover scene. The Minnaert k-value is derived from the digital Landsat data using a regression equation, and provides a measure of the geometry controlling surface reflection. Most natural surfaces have k-values between zero and one (Smith et al, 1980), with a value of one indicating a Lambertian, or perfectly diffuse reflecting surface, and smaller values of k indicating a specular reflecting surface (Justice and Holben, 1979). This investigation was undertaken partly to demonstrate that snow acts as a diffuse reflector of light (as in Byton, 1969) and to model the reflectance of a Landsat snow-cover scene for determining the sensitivity of the model with respect to detecting small slope differences present in the terrain.

Scene brightness is calculated from the Minnaert (1941) function shown below:

$$L = k \cos^k i \cos^{k-1} e, \tag{1}$$

where

L = satellite scene radiance

k = constant

i = effective incident angle

e = exitance angle

k = estimated parameter.

The value of k is estimated through a regression of the linearized equation (1). The derivation is after Smith et al, (1980), as paraphrased by Eyton (1989):

$$L = \frac{k \cos^{k-1} i \cos e}{\cos e},$$ (2)

or

$$L \cos e = k \cos^k i \cos^k e.$$ (3)

Taking the logarithm of each side of the equation gives the linearized transformation:

$$\log(L \cos e) = \log(k) + k \log(\cos i \cos e).$$ (4)

Letting

$Y = \log (L \cos e)$,

$X = \log (\cos i \cos e)$,

$b = \log (k)$,

then

$Y = b + kx$.

The regression of Y on X yields the values of b and k.

The effective incident angle and exitance angle are determined from the geometry of the sun's position relative to the terrain and given by:

$$\cos i = \cos \theta_s \cos \theta_t + \sin \theta_s \sin \theta_t \cos(\phi_s - \phi_t),\tag{5}$$

$$\cos e = \cos \theta_t,\tag{6}$$

where

θ_s = slope zenith angle ($90° -$ elevation of the sun)

θ_t = slope facet magnitude,

ϕ_s = solar azimuth angle,

ϕ_t = slope facet azimuth.

To estimate the k-value for snow-covered topography in the Landsat study image, 57 measurements of slope magnitude and azimuth were obtained from 21 National Topographic System (NTS) map sheets scale 1:50,000. Slope samples (slope rise divided by slope run) were calculated by measuring approximately equidistant contours at 7,620 metre intervals (representing even, continuous slopes) of at least 450 metres in length; the run measurement was orthogonal to the contours. Mean run length was approximately 1227 metres resulting in an average slope of approximately 1.17 degrees for the 57 observations. Slope azimuths varied from one to 343 degrees.

Sixteen readily identified control points were located using Universal Transverse Mercator (UTM) coordinates on the NTS map sheets and by row and column pixel locations from the image data. An affine coordinate transformation was then executed

to convert the 57 slope sample UTM coordinates to row and column locations. A 7-row by 9-column pixel subset oriented about the slope length centre was extracted from all four Landsat image bands. Ground length of the image subset (738 metres) was shorter than the average run length (1227 metres) measured on the maps to ensure accurate representation of the ground area. From these subsets the mean radiance value was calculated for each 63 pixel matrix, excluding all pixels with grey levels representing snow-free or tree-covered areas.

Table 3 lists the slope magnitudes, slope azimuths and mean grey level values for the 57 sampled observations. Coefficients of determination (r^2), h-constants (h-intercepts) and k-values (slope of the linearized regression line) derived from the regression analysis from all four bands are given in Table 4. These findings corroborate Byrne's (1989) study showing that snow is a diffuse reflector of light at low solar elevations and that Minnaert k-values increase with increasing spectral wavelength. Although the calculated k-values from bands 5,6 and 7 exceed 1.0 (Table 4) due to estimation error inherent in the regression equation, the k-values show that Lambertian reflection (k=1.0) for a snow-covered scene is a reasonable assumption. The Minnaert function in equation 1 simplifies to:

$$L = h \cos i,$$ (7)

where

L = satellite scene radiance,

h = constant,

i = effective incident angle.

Table 3. NTS Map Slope Components and Band 6 Scene Radiance Measurements

Quarter	Slope Magnitude (°)	Slope Azimuth (°)	Mean Gray Level (Value, L)
1	0.57	62.1	105
2	2.85	32.6	103
3	2.42	32.1	125
4	0.52	325.0	115
5	4.26	215.0	115
6	1.27	143.3	120
7	1.94	12.5	123
8	1.26	247.6	124
9	2.42	68.5	135
10	1.94	64.5	125
11	1.94	143.4	124
12	2.62	34.4	119
13	1.38	9.0	122
14	0.57	1.0	123
15	0.70	137.0	137
16	0.73	323.6	135
17	1.58	32.6	133
18	1.58	68.6	137
19	1.94	68.6	137
20	1.73	208.0	127
21	1.26	147.0	130
22	1.58	147.0	127
23	0.58	325.0	145
24	0.58	181.4	124
25	1.58	68.4	135
26	1.67	117.4	137
27	1.58	123.4	136
28	1.30	123.0	145
29	1.11	123.0	145
30	2.10	204.0	133
31	2.26	323.3	137
32	0.58	172.3	134
33	0.58	183.7	133
34	1.67	32.3	142
35	0.50	324.3	133
36	0.58	32.3	133
37	0.58	323.6	141
38	1.46	32.6	141
39	0.58	123.6	133
40	0.58	123.6	133
41	1.58	123.6	133
42	0.58	323.6	133
43	0.58	323.6	146
44	0.58	32.6	135
45	1.58	32.6	133
46	1.58	117.6	134
47	0.58	123.6	133
48	0.58	323.6	133
49	0.58	32.6	133
50	0.58	181.1	143
51	0.58	325.3	133
52	1.58	32.2	133
53	1.58	323.3	107

Table 4. Minmart Function Regression Results

Parameters	B4	B5	B6	B7
r^2	0.4921	0.5743	0.6543	0.6777
b-constant	2.6321	2.7146	2.8164	0.6724
k-value	0.9349	1.0808	1.1162	1.2075

Image Brightness Thresholding

Modelling the reflectance of snow-cover scene image data allowed for development of a method to estimate grey level values for flat terrain and the low-relief sun-facing and sun-opposing slopes in a subscene. Table 5 shows the predicted grey level values for the regression of the linearized Minnaert function given in equation 4; Band 6 regression parameters (Table 4) were used because of the relatively high r^2 value associated with the only MSS infrared channel utilizing a full dynamic range of brightness values. Plate 17 shows a binary, thresholded image subset with threshold pixel grey level values of 0 to 129 displayed as white, and values of 130 or greater shown as black. Black pixels (grey level values≥129) represent sun-facing slopes. White pixels (grey level values<129) indicate sun-opposing slopes. By assigning a black tone to the sun-facing slopes a crude hillshaded model (Plate 17) enhancing the terrain, with the illumination source located in the northwest, was created (Eyton, 1989). This technique was used to produce a three-tone thresholded image. Plate 18 is an image of the findings subscene in which light grey pixels (grey level values ≥122 and ≤137) represent slopes up to one degree (considered to be representative of flat terrain). Black pixels (grey level values >137) indicate sun-facing slopes greater than one degree, and white pixels (grey level values <122) show sun-opposing slope facets greater than one degree.

Table 5. Predicted Band 6 Grey Level Values for Sun-Facing and Sun-Opposing Slopes

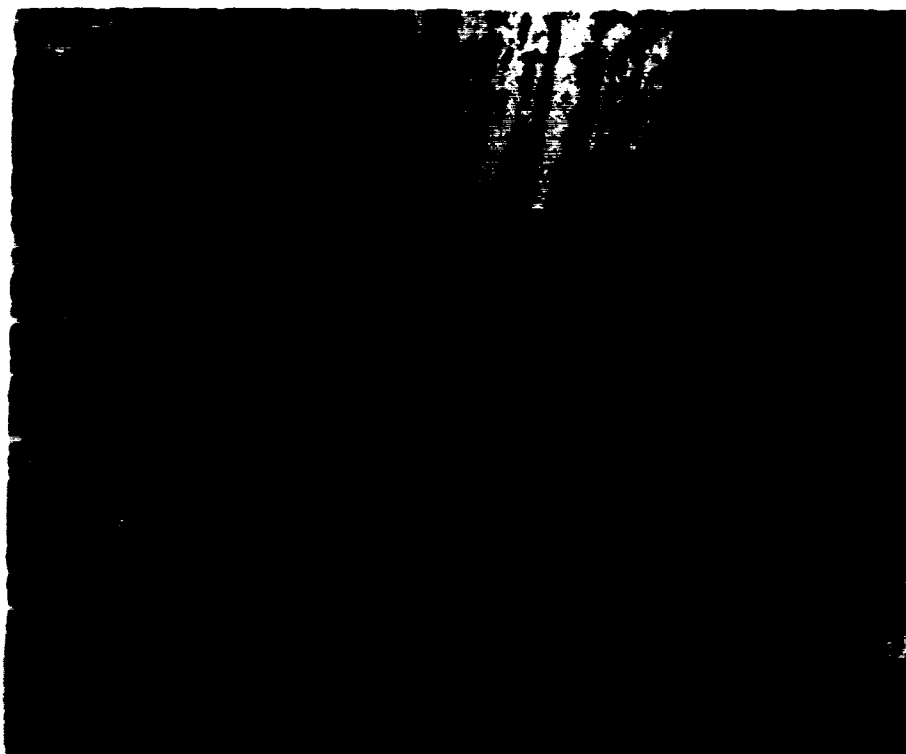| Slope Magnitude (degrees)	Grey Level Value	
	Sun-facing	Sun-opposing
0.0	129	129
0.1	130	129
0.2	131	128
0.3	131	127
0.4	132	126
0.5	133	126
0.6	134	125
0.7	134	124
0.8	135	123
0.9	136	123
1.0	137	122
1.1	137	121
1.2	138	120
1.3	139	120
1.4	140	119
1.5	140	118
1.6	141	117
1.7	142	117
1.8	142	116
1.9	143	115
2.0	144	114

Plate 17. A binary thresholded image of the large-scale fluting indicating sun-facing (black pixels) and sun-opposing (white pixels) slopes.
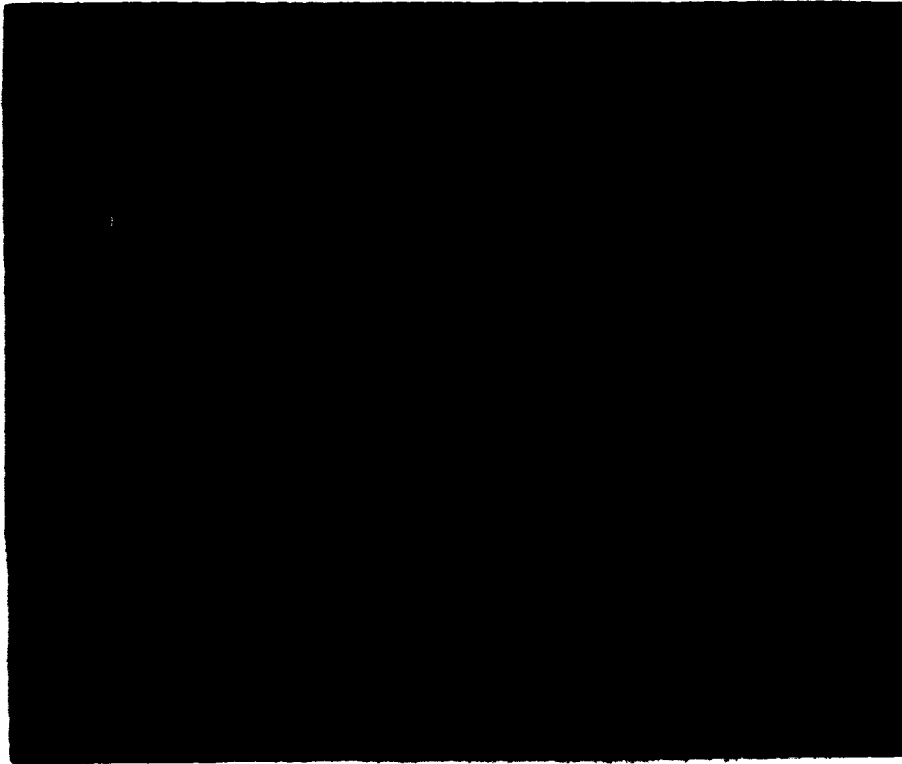
Plate 28. A three-zone thresholded image of the large-scale findings showing "flat" surfaces as light grey pixels, steeper sun-facing slopes as black and sun-opposing slopes as white.

Reflectance Model Sensitivity

In order to examine the sensitivity of the reflectance model, the regression parameters for MSS band 7 were used, as this data set provided the highest r^2 value for the initial reflectance modelling. Using the Minnaert function (equation 4) and the regression parameters for the band 7 data (Table 4), a difference of two grey level values between ___ sun-facing and sun-opposing slopes (see Figure 3) resulted from an angular difference of 0.28 degrees for the two opposing slope facets.

The same estimate (equation 4) can be calculated for features that have different slope orientations relative to the sun. The features shown in Plate 13 have an approximate 21/201 degree (NNE-SSW) trend. Figure 4 shows the approximate angles of the sun-facing and sun-opposing fluting slope facets and sun azimuth angle at the time the image was acquired. Table 6 shows predicted grey level values for slope facets of the flutings. Inspection of the raw data from the band 7 subset of the fluting area show average sun-facing grey level values of approximately 90 and sun-opposing grey level values of about 70. Table 6 indicates that sun-facing slopes with grey level values of 90 correspond to a slope magnitude of 1.8 degrees, while sun-opposing slopes with grey level values of 70 represent slopes of 2.2 degrees. These values correspond in magnitude to casual field estimates for the fluting slope values.
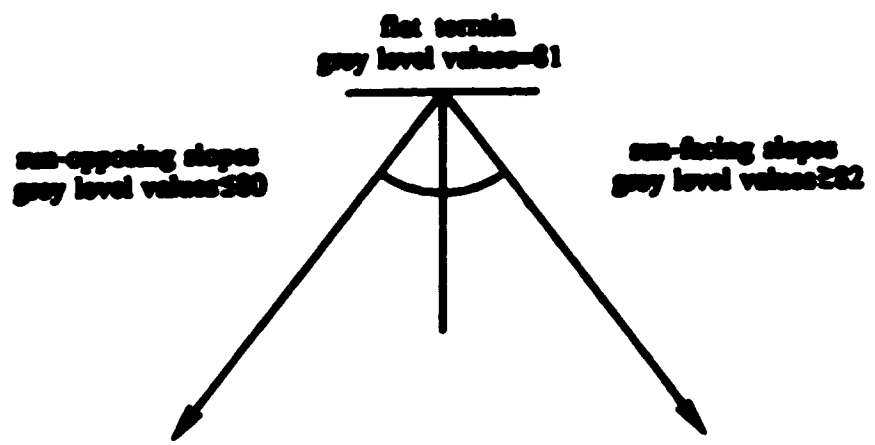
Figure 3. Two sun-facing and sun-opposing slope faces and angular separation between the slopes.

approximate fluting trend
21°

sun-opposing fluting slopes
291°

sun-facing fluting slopes
111°

solar azimuth
154.5°

201°
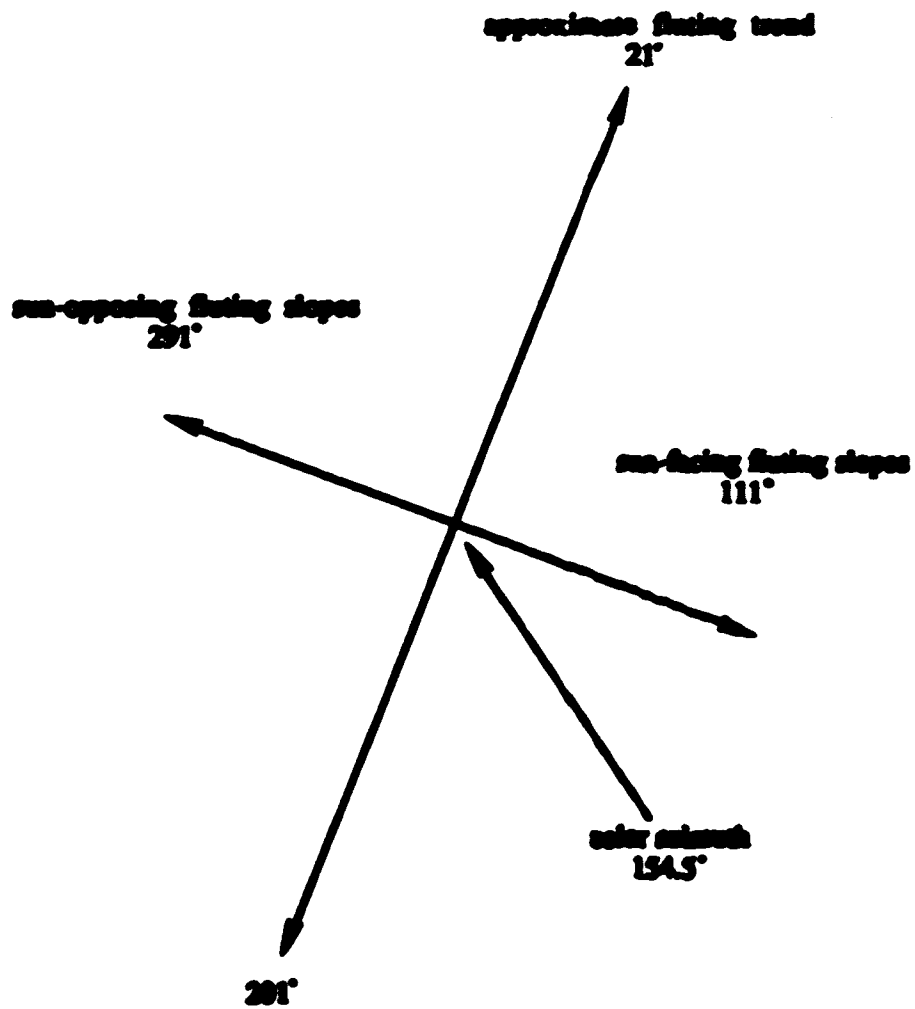
Figure 4. Fluting trend, sun-facing and sun-opposing slope facet angles, and solar azimuth angle.

Table 6. Predicted Band 7 Grey Level Values for Sun-Facing and Sun-Opposing
Fluting Slope Facets

	Grey Level Values	
Slope Magnitude (degrees)	Sun-facing	Sun-opposing
0.0	81	81
0.2	82	80
0.4	83	79
0.6	84	78
0.8	85	77
1.0	86	76
1.2	87	75
1.4	88	74
1.6	89	73
1.8	90	72
2.0	92	71
2.2	93	70
2.4	94	69
2.6	95	68
2.8	96	67
3.0	97	66

Sensitivity of the model indicates that solar azimuth, at the time of image acquisition, like solar elevation, is critical for the creation of brightness differences between slopes at varying orientations relative to the sun. Plate 19 is a photograph of a Landsat snow-cover image acquired with the Thematic Mapper (TM) sensor November 5, 1984. The contrast between fluting ridges and troughs appears to have been eliminated by their slightly more parallel alignment to the sun (solar azimuth=159.60 degrees) relative to the January 14, 1984 MSS solar azimuth angle (154.55 degrees).

Plate 13. Photograph of a November 5, 1984, Landsat TM snow-cover scene. Findings are no longer discernible with a solar azimuth of 150.6 degrees. Solar elevation is 28.41 degrees.

V. CONCLUSIONS

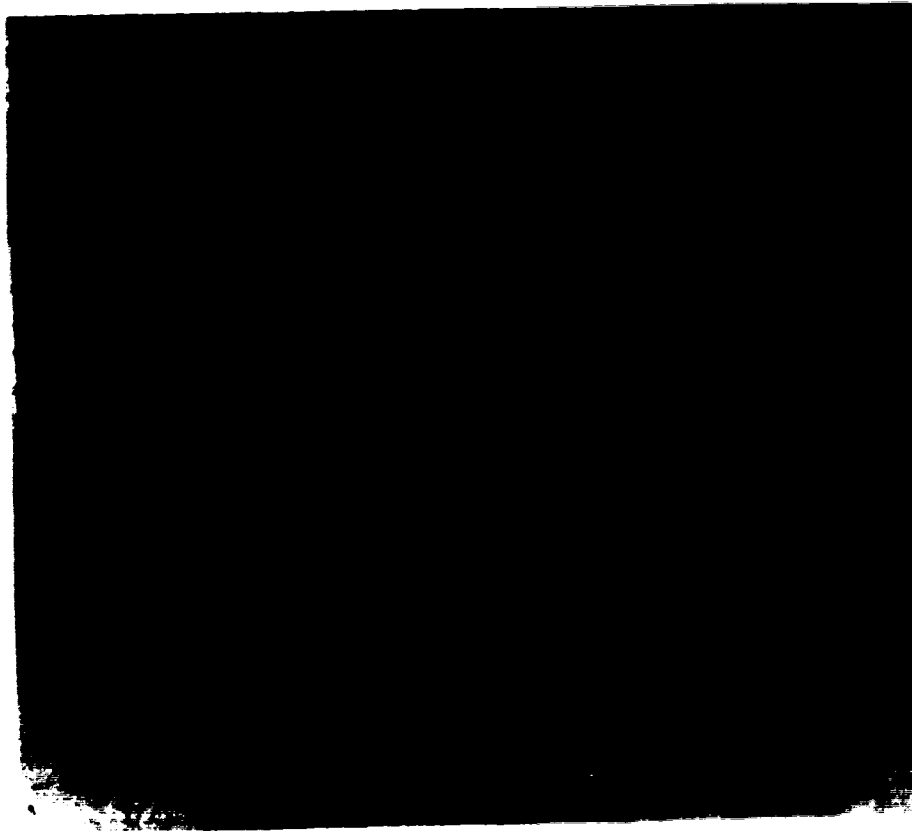Digital snow-cover imagery was used to enhance low-relief topographic expression in a Landsat MSS scene. The reflectance, or light-scattering properties of snow-covered terrain illuminated at a low solar elevation produced image brightness differences from surface slope differences (sun-facing versus sun-opposing) as small as 0.28 degrees. Examination of a Minnaert-based photometric function showed that increased spectral wavelengths produced greater differences in radiance between sun-facing and sun-opposing low-relief slopes. These slight but very significant differences were digitally processed to create enhanced image subscenes that revealed discrete but extensive glacigenic landforms in south-central Alberta, and to estimate very slight slope variations based on the image brightness differences.

The use of digital snow-cover imagery to enhance the subtle topographic expression visible in this study was found to be dependent upon several critical factors, including the following:

1. Solar elevation angle: slight image brightness differences produced from subtle variations in topography in the image data are more pronounced at lower sun elevations. Image data acquired as close as possible to the winter solstice (December 20-22 in the northern hemisphere) should be obtained for analysis.

2. Solar azimuth angle: sensitivity of the model indicates that solar azimuth is also critical for creation of brightness differences between slopes at varying azimuths relative to the sun. Enhancement of slopes is increased naturally with sun azimuths

that are more perpendicular to the slope facets.

3. Absence of coniferous or deciduous trees obscuring the snow cover: both coniferous and leafless deciduous tree stands located within the image data obscured the snow-covered terrain.

4. Homogeneous covering of snow: the ubiquity of snow-cover, rather than minor differences of snow depths (as reported by weather stations within the study area on the day of scene acquisition) enhanced topographic expression in the snow-cover scene.

5. Shadow: the relatively extreme topography of some areas within the image, and the low solar elevation during image acquisition, resulted in dark shadows on some northwest-facing slopes that obscured snow-covered surfaces. The ability to determine relative brightness differences between sun-opposing slopes and sun-facing slopes was lost in these instances.

Related, future areas of research might focus on:

1. Modelling the reflectance of snow-covered surfaces using a diffuse (cos i) Lambertian reflectance model: the assumption that snow is a perfectly diffuse reflecting surface has been validated in this study.

2. Examination of Landsat Thematic Mapper imagery data: increased spatial resolution (30 metres x 30 metres) may resolve smaller, discrete landforms in snow-cover image data.

3. Comparison with SAR (Synthetic Aperture Radar) and SLAR (Side-Looking Airborne Radar) imagery: detection of large-scale landforms using low look-angle

radar images should be comparable to a snow-cover scene.

The geomorphological utility of enhanced snow-cover imagery as an investigative and interpretive tool was demonstrated in this study. Vastly improved delineation of partially mapped glacial meltwater channel networks (Shetsen, 1990) and detection of previously undiscovered large-scale features, illustrate the value of enhanced snow-cover imagery in recognizing regional-scale landform suites not readily apparent from field investigation or necessarily visible on conventional aerial photographs. Image processing of Landsat data provides enhanced digital images useful for mapping of these topographic elements at a variety of scales. Mosaics of full Landsat scenes, at a 1:1,000,000 scale, would provide investigators with an efficient and accurate base on which to focus comprehensive, field-oriented geomorphological investigations.

References

Beaty, C.B., 1975. The Landscapes of Southern Alberta: A Regional Geomorphology. University of Lethbridge Production Services, 69-76.

Burns, J.A., and Young, R.R., 1988. Stratigraphy and palaeontology of the Hand Hills region. Occasional Paper of the Tyrrell Museum of Palaeontology, 9.

Campbell, I.A., 1987. Badlands of Dinosaur Provincial Park, Alberta. The Canadian Geographer, 31: 82-87.

Crooks, L., 1988. The integration of digital satellite imagery and digital landform models for the analysis and mapping of Dall's Sheep (Ovis dalli dalli) habitat in the Yukon Territory. Unpublished M.Sc. thesis, University of Alberta, 45 pp.

Davis, J.C., 1986. Statistics and Data Analysis in Geology. John Wiley and Sons, Inc., New York, 527-546.

Dyke, A.S., and Prest, V.K., 1987. Late Wisconsinan and Holocene history of the Laurentide ice-sheet. Geographie physique et Quaternaire, XLI(2): 237-263 and maps.

Evans, A.H., 1990. Manipulation of relief in a Thematic Mapper scene of mountainous terrain in the Yukon. Unpublished M.Sc. thesis, University of Alberta, 58 pp.

Ryton, J.R., 1989. Low-relief topographic enhancement in a Landsat snow-cover scene. Remote Sensing of Environment, 27 (105): 105-118.

Gravenor, C.P., and Munday, W.A., 1958. Glacial features in central and northern Alberta. American Journal of Science, 256: 715-728.

Horn, B.K.P., 1982. Hillshading and the reflectance map. Geo-Processing, 2: 65-146.

Irish, E.J.W., 1967. Drumheller Geology Map 5-1967, 1:253,440. Geological Survey of Canada.

Jacques, D.R., 1982. Landsat mapping of snow-cover to identify critical wildlife winter range. Alberta Remote Sensing Centre Publication No. 82-3, Edmonton, Alberta, 11 pp.

Jones, N.K., 1982. The formation of glacial flutings in east-central Alberta. In: R. Davidson-Arnott, W. Nickling, and B.D. Fahey (editors), Research in Glacial, Glacio-fluvial and Glacio-lacustrine Systems. Proceedings of the 6th Guelph Symposium on Geomorphology, 1980. Geo Books, Norwich, England, 49-70.

Justice, C., and Holben, B., 1979. Examination of Lambertian and non-Lambertian models for simulating the topographic effect on remotely sensed data. NASA TM 80557, Goddard Space Flight Center, Greenbelt, M.D., 20 pp.

Justice, C.O., Wharton, S.W., and Holben, B.N., 1981. Application of digital terrain data to quantify and reduce the topographic effect on Landsat data. International Journal of Remote Sensing, 2(3): 213-220.

Kriebel, K.T., 1978. Measured spectral bidirectional reflection properties of four vegetated surfaces. Applied Optics, 17(2): 253-263.

Lillesand, T.M., and Kiefer, R.W., 1987. Remote Sensing and Image Processing. John Wiley and Sons, Inc., New York, 610-636.

Lucchita, B.K., Bowell, K.L.E., Edison, E.M., and Ferguson, H.M., 1987. Multispectral Landsat Images of Antarctica. U.S. Geological Bulletin 1696, 21 pp.

Minnaert, M., 1941. The reciprocity principle in lunar photometry. Journal of Astrophysics, 93: 403-410.

Mooers, S.R., Clayton, L., Hooke, R.L., Fenton, M.M., Andriashek, L.D., 1980. Glacier-bed landforms of the prairie region of North America. Journal of Glaciology, 25(93): 457-476.

Morrison, R.B., 1976. Enhancement of topographic features by snow cover. In: R.S. Williams, Jr. and W.D. Carter, (editors), ERTS-1, A New Window on Our Planet. U.S.G.S. Professional Paper, 929: 72-75.

Pettapiece, W.W., 1986. Physiographic Subdivisions of Alberta. Alberta Agriculture map, 1:1,500,000.

Ramachandran, V.S., 1988. Perceiving shape from shading. Scientific American, 259(2): 76-83.

Rains, R.B., Kvill, D.R., and Shaw, J., 1990. Evidence and some implications of coalescent Cordilleran and Laurentide glacier systems, Western Canada. In: P.J. Smith and E.L. Jackson, (editors), A World of Real Places: Essays in Honour of W.C. Wonders, Edmonton, University of Alberta, Department of Geography Occasional Publications, 147-161.

Richards, J.A., 1986. Remote Sensing Digital Image Analysis. Springer Overlag, Berlin, 83-103.

Shaw, J., 1975. The formation of glacial flutings. In: R.P. Suggate and M.M. Cresswell (editors), Quaternary Studies. The Royal Society of New Zealand, Wellington, 253-258.

Shaw, J., 1980. Drumlins and large-scale flutings related to glacier folds. Arctic and
Alpine Research, 12(3): 287-298.

Shaw, J., and Kvill, D.R., 1984. A glaciofluvial origin for drumlins of the Livingston
Lake Area, Saskatchewan. Canadian Journal of Earth Sciences, 21: 1256-1267.

Shaw, J., and Sharpe, D.R., 1987. Drumlin formation by subglacial meltwater erosion.
Canadian Journal of Earth Sciences, 24: 2316-2322.

Shaw, J., Kvill, D.R., Rains, R.B., 1989. Drumlins and catastrophic subglacial floods.
Sedimentary Geology, 62: 177-202.

Shetsen, I., 1987. Quaternary geology, Southern Alberta. Alberta Research Council
Map, 1:500,000.

Shetsen, I., 1990. Quaternary geology, Central Alberta. Alberta Research Council Map,
1:500,000.

Smith, D.G., 1987. Landforms of Alberta. Alberta Remote Sensing Centre Publication
No. 87-1, 104 pp.

Smith, H.T.U., 1943. Aerial Photographs and Their Applications. D. Appleton-Century
Company, Inc., New York, 54-57.

Smith, H.T.U., 1948. Giant glacial grooves in northwest Canada. American Journal of
Science, 246(8): 503-514.

Smith, J.A., Lin, T.L., and Ranson, K.J., 1980. The Lambertian assumption and
Landsat data. Photogrammetric Engineering and Remote Sensing, 46(9): 1183-
1189.

Stalker, A. MacS., 1960 a. Surficial geology of the Red Deer-Stettler map area,

Alberta. Geological Survey of Canada Memoir, 306: 1-140, and maps.

Stalker, A. MacS., 1960 b. Ice-pressed drift forms and associated deposits in Alberta. Geological Survey of Canada Bulletin, 57: 1-38, and maps.

Stalker, A. MacS., 1973. Surficial geology of the Drumheller area, Alberta. Geological Survey of Canada Memoir, 370: 1-122.

Tsui, P.C., Cruden, D.M., and Thomson, S., 1989. Ice- thrust terrains and glaciotectonic settings in central Alberta. Canadian Journal of Earth Sciences, 26: 1308-1318.

Wobber, F.J., and Martin, K.R., 1973. Exploitation of ERTS-imagery utilizing snow enhancement techniques. Symposium on Significant Results Obtained from the Earth Resources Technology Satellite-1, NASA SP-327, 1: 345-352.

Wobber, F.J., and Martin, K.R., 1974. Utilization of Snow Enhancement Techniques for Acquisition of Geological and Geo-Environmental Information from ERTS Imagery, Earth Satellite Corporation, Washington, D.C., unpublished manual, 29 pp.

von Gaza, P., 1989. Image enhancement for mineral exploration. Unpublished M.Sc. thesis, University of Alberta, Edmonton, 80 pp.